SCIENCE CHINA
Information Sciences

• Supplementary File •

Quantum illumination with post-processing of displacement and anti-displacement operations

ShengLi ZHANG[1]

[1] *School of Physics, Beijing Institute of Technology, Beijing,*100081*, China,*

Appendix A Quantum illumination and basic formulation

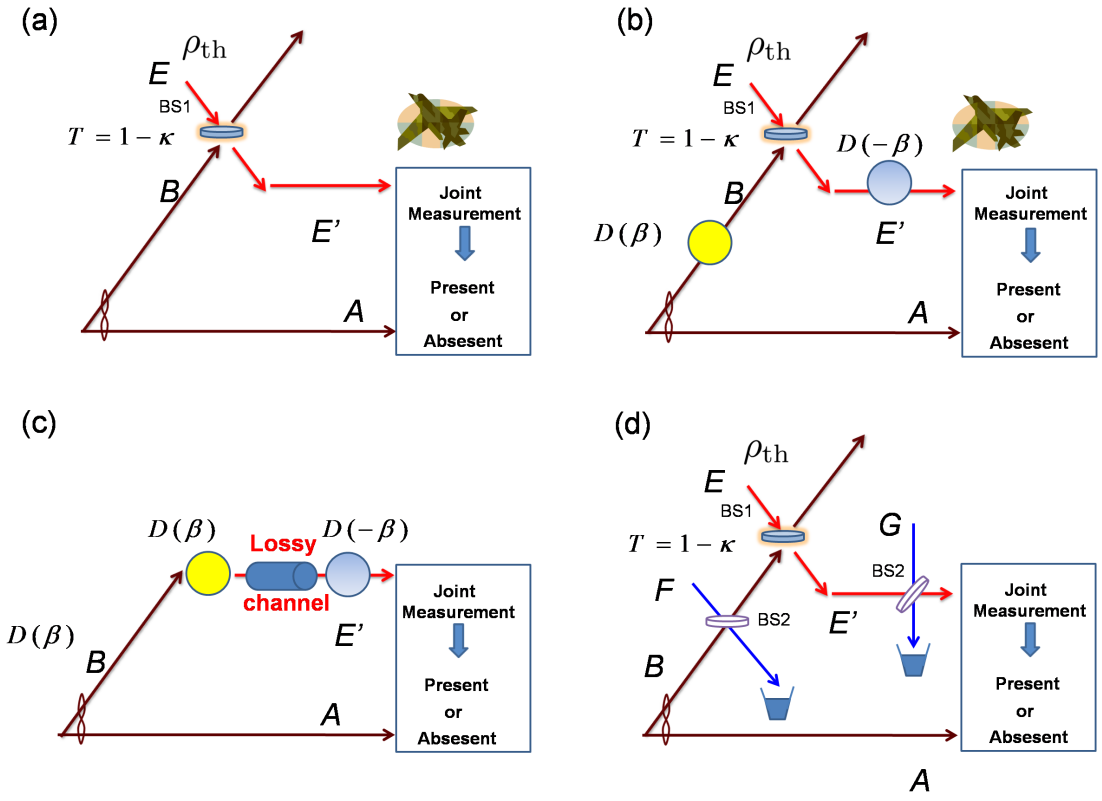

Figure A1 (a) Target detection with the two-mode squeezed state. (b) Enhanced target detection via displacement and anti-displacement operations. On considering a displacement amplitude of zero, this scheme is reduced to the traditional quantum illumination scheme. (c) Channel model of the interaction with the target. (d) Practical implementation of displacement operation using a beam splitter with transmittance T_0, ancillary coherent states $|\beta_0\rangle$, and $|-\beta_0\rangle$ in F and G modes. BS1 is a beam splitter with transmittance $T=1-\kappa$; it is used to model the target. Trash boxes denote the discarding operation.

The scheme of quantum illumination is presented in Fig. A1(a). A two-mode squeezed state $\rho_{AB}=|\psi\rangle_{TMSS}\langle\psi|$ serves as the source with

$$|\psi\rangle_{TMSS}=\sqrt{1-\lambda^2}\sum_{n=0}^{\infty}\lambda^n|n,n\rangle,\lambda=\tanh(r). \tag{A1}$$

A and B are the idle and signal modes, respectively. The target with reflectivity κ is modeled with a beam splitter of transmittance $T=1-\kappa$. E mode is a single-mode thermal state $\rho_{\rm th}=(1-\mu)\sum_{n=0}^{\infty}\mu^n|n\rangle\langle n|$ (average number of photons: $N_B=\frac{\mu}{1-\mu}$) for

Email: zhangshengli@bit.edu.cn

simulating thermal noise. The outgoing mode E' after the coupling of the beam-splitter is collected using a detector; E' and A are measured jointly to determine the existence of the target. If the target is present, $\rho_{E'A}$ is obtained at the receiver. However, if the target is absent, the product state $\rho_E \otimes \rho_A = \rho_{E'A}(\kappa = 0)$ is obtained, where $\rho_A = \mathrm{Tr}_B[\rho_{AB}]$ is the reduced density matrix in the optical mode A. Generally, joint quantum measurements are more effective for quantum state discrimination; this explains the higher efficiency of quantum illumination, as compared with that of classical state illumination.

Here, we propose using the sequential displacement operation $D(\beta)$ and anti-displacement operation $D(-\beta)$ before and after the interaction of B with the target, respectively, in order to improve the performance of target detection (Fig. A1(b)). The interaction of B with the target can be considered as a quantum channel $\mathcal{E}$, such that $\mathcal{E} : \rho_B \rightarrow \mathrm{Tr}[U_{EB}(\rho_E \otimes \rho_B)U_{EB}^{\dagger}]$. A plot of the equivalence to the channel is shown in Fig.A1 (c). The novelty of this research lies in the fact that a displacement operation was performed before the channel and an anti-displacement operation was performed after the channel. By setting $\beta = 0$, the original quantum illumination can be recovered, as shown in Fig. A1(a). It should be noted that, regardless of the presence or absence of the target, the auxiliary displacement and anti-displacement operations are always performed. The subsequent sections detail how these two operations help improve the performance of quantum illumination.

Quantitatively, the performance of target detection is evaluated based on the probability of erroneous inferences of the existence of the target. This is equivalent to the discrimination between two mixed states, i.e., $\rho_{E'A}(\kappa = 0)$ and $\rho_{E'A}(\kappa = \kappa_t)$, where κ_t is the reflectivity of the target. In the absence of prior information regarding the target, the a priori probability is assumed as follows:

$$P(\kappa = 0) = P(\kappa = \kappa_t) = \frac{1}{2}. \tag{A2}$$

Thereafter, we define

$$\rho_{E'A}^{(0)} = \rho_{E'A}\big|_{\kappa=0}, \rho_{E'A}^{(1)} = \rho_{E'A}\big|_{\kappa=\kappa_t}. \tag{A3}$$

According to the theory of optimal quantum state discrimination, the minimum error probability is [1, 2]

$$P_{\mathrm{err}} = \frac{1}{2}\left(1 - \frac{1}{2}||\rho_{E'A}^{(0)} - \rho_{E'A}^{(1)}||\right), \tag{A4}$$

where $||\gamma|| = \mathrm{Tr}(\sqrt{\gamma^{\dagger}\gamma}) = \sum_i s_i(\gamma)$, and $s_i(\gamma)$ is the absolute value of the eigenvalue [1]. In practice, $\kappa \ll 1$ is considerably small; therefore, a large number (i.e., M) of copies of $\rho_{E'A}$ are required to achieve an infinitesimal error probability. This is defined as

$$P_{\mathrm{err,M}} = \frac{1}{2}\left(1 - \frac{1}{2}||{\rho_{E'A}^{(0)}}^{\otimes M} - {\rho_{E'A}^{(1)}}^{\otimes M}||\right). \tag{A5}$$

When M is considerably large, the precise evaluation of P_{err} is significantly difficult; the quantum Chernoff bound (QCB) is typically employed to estimate $P_{\mathrm{err,M}}$ [3]:

$$P_{\mathrm{err,M}} \leqslant P_{\mathrm{QCB}}^{M} = \frac{1}{2}Q_{\mathrm{E'A}}^{M}, \tag{A6}$$

where

$$Q_{\mathrm{E'A}} = \min_{0 \leqslant s \leqslant 1} \mathrm{Tr}[\rho_{E'A}^{(1)s}\rho_{E'A}^{(0)1-s}]. \tag{A7}$$

The scheme of quantum illumination with a smaller $Q_{\mathrm{E'A}}$ provides a considerably lower $P_{\mathrm{err,M}}$.

Appendix B Quantum state evolution under illumination

Appendix B.1 Low-noise conditions

We first analyze the state evolution in a few-photon subspace spanned by $\{|0\rangle, |1\rangle\}$. This is a good approximation when the average number of photons is significantly small and the population of the higher-photon number subspace can be neglected.

First, we consider the case of quantum illumination without the displacement or anti-displacement operations. The state in mode $E - A - B$ can be expressed as

$$\begin{aligned}\rho_E \otimes |\psi\rangle_{AB}\langle\psi| \quad &= (1-\mu)(1-\lambda^2)\left[|0\rangle_E\langle 0| + \mu|1\rangle_E\langle 1|\right] \\ &\otimes \left[|00\rangle_{AB} + \lambda|11\rangle_{AB}\right]\left[{}_{AB}\langle 00| + \lambda_{AB}\langle 11|\right].\end{aligned} \tag{B1}$$

The coupling of the beam splitter between modes E and B can be written as $U_{\mathrm{ES}}(T) = \exp[\theta(\hat{a}_E\hat{a}_B^{\dagger} - \hat{a}_E^{\dagger}\hat{a}_B)]$, $\theta = \arctan\left(\sqrt{(1-T)/T}\right)$, where $T = 1 - \kappa$. The reduced density matrix of E' and A is obtained by taking a partial trace over the mode B, i.e.,

$$\rho_{E'A} = \mathrm{Tr}_B\left[U_{\mathrm{EB}}\left(\rho_E \otimes |\psi_{AB}\rangle\langle\psi_{AB}|\right)U_{\mathrm{EB}}^{\dagger}\right] \tag{B2}$$

$$\begin{aligned}&= \frac{1}{1+\mu+\lambda^2\left(1+(1-2\kappa)^2\mu\right)}\left\{(1+\kappa\mu)|00\rangle\langle 00|\right. \\ &-\sqrt{\kappa}\lambda(1+(2\kappa-1)\mu)\left(|00\rangle\langle 11| + |11\rangle\langle 00|\right) \\ &+(1-\kappa)\lambda^2|01\rangle\langle 01| + \mu(1-\kappa)|10\rangle\langle 10| \\ &\left.+\lambda^2(\kappa+\mu-4\kappa\mu+4\kappa^2\mu)|11\rangle\langle 11|\right\}.\end{aligned} \tag{B3}$$

Similarly, the reduced density matrix for the case wherein the displacement and anti-displacement operations are employed can be derived as follows:

$$\widetilde{\rho}_{E'A} = \mathrm{Tr}_B \left[U_{\mathrm{EB}} \left(\rho_E \otimes |\psi'\rangle\langle\psi'| \right) U_{\mathrm{EB}}^{\dagger} \right], \tag{B4}$$

$$\rho_{E'A}(\beta) = (D(-\beta) \otimes I) \widetilde{\rho}_{E'A} (D(-\beta)^{\dagger} \otimes I), \tag{B5}$$

where $|\psi'\rangle = I \otimes D(\beta)|\psi\rangle_{TMSS}$, and $D(\beta) = e^{\beta \hat{a}^{\dagger} - \beta^* \hat{a}}$ is the displacement operator.

Through direct calculation, the density matrix $\rho_{\mathrm{E'A}}(\beta)$ in the 0-1 photon subspace can be expressed in the basis $\{|00\rangle, |01\rangle, |10\rangle, |11\rangle\}$, as follows:

$$\rho_{\mathrm{E'A}}(\beta) = \begin{pmatrix} \rho_{11} & \rho_{12} & \rho_{13} & \rho_{14} \\ \rho_{21} & \rho_{22} & \rho_{23} & \rho_{24} \\ \rho_{31} & \rho_{32} & \rho_{33} & \rho_{34} \\ \rho_{41} & \rho_{42} & \rho_{43} & \rho_{44} \end{pmatrix}, \tag{B6}$$

where

$$\rho_{11} = \frac{(1+\kappa\mu)Cos[\beta]^2 + \lambda\left(\lambda - \kappa\lambda - \sqrt{\kappa}(-1+\mu) + 2\kappa^{3/2}\mu\right) Sin[\beta]^2}{1+\mu+\lambda^2\left(1+(1-2\kappa)^2\mu\right)}, \tag{B7}$$

$$\rho_{12} = \frac{Sin[\beta]\left(\left(1+(-1+\kappa)\lambda^2+\kappa\mu\right) Cos[\beta] + \sqrt{\kappa}\lambda(1+(-1+2\kappa)\mu) Sin[\beta] Tan[\beta]\right)}{1+\mu+\lambda^2\left(1+(1-2\kappa)^2\mu\right)}, \tag{B8}$$

$$\rho_{13} = \frac{Sin[\beta]\left(\left(\mu - \kappa\mu + 2\kappa^{3/2}\lambda\mu + \sqrt{\kappa}(\lambda-\lambda\mu)\right) Cos[\beta] + \lambda^2\left(\kappa+\mu-4\kappa\mu+4\kappa^2\mu\right) Sin[\beta] Tan[\beta]\right)}{1+\mu+\lambda^2\left(1+(1-2\kappa)^2\mu\right)}, \tag{B9}$$

$$\rho_{14} = -\frac{\sqrt{\kappa}\lambda(1+(-1+2\kappa)\mu)\mathrm{Cos}[\beta]^2 + \left(4\kappa^2\lambda^2\mu + \left(-1+\lambda^2\right)\mu + \kappa\left(\lambda^2+\mu-4\lambda^2\mu\right)\right)\mathrm{Sin}[\beta]^2}{1+\mu+\lambda^2\left(1+(1-2\kappa)^2\mu\right)}, \tag{B10}$$

$$\rho_{21} = \frac{\left(1-\lambda^2+\sqrt{\kappa}\lambda(-1+\mu) - 2\kappa^{3/2}\lambda\mu + \kappa\left(\lambda^2+\mu\right)\right) Cos[\beta] Sin[\beta]}{1+\mu+\lambda^2\left(1+(1-2\kappa)^2\mu\right)}, \tag{B11}$$

$$\rho_{22} = \frac{-(-1+\kappa)\lambda^2 Cos[\beta]^2 + \left(1+\sqrt{\kappa}\lambda(-1+\mu) + \kappa\mu - 2\kappa^{3/2}\lambda\mu\right) Sin[\beta]^2}{1+\mu+\lambda^2\left(1+(1-2\kappa)^2\mu\right)}, \tag{B12}$$

$$\rho_{23} = -\frac{\left(\sqrt{\kappa}\lambda(-1+\mu) - 2\kappa^{3/2}\lambda\mu + 4\kappa^2\lambda^2\mu + \left(-1+\lambda^2\right)\mu + \kappa\left(\lambda^2(1-4\mu)+\mu\right)\right) Sin[\beta]^2}{1+\mu+\lambda^2\left(1+(1-2\kappa)^2\mu\right)}, \tag{B13}$$

$$\rho_{24} = \frac{Sin[\beta]\left(\lambda\left(\sqrt{\kappa}(-1+\mu) - 2\kappa^{3/2}\mu + \lambda\mu + 4\kappa^2\lambda\mu + \kappa(\lambda-4\lambda\mu)\right) Cos[\beta] - (-1+\kappa)\mu \mathrm{Sin}[\beta]\mathrm{Tan}[\beta]\right)}{1+\mu+\lambda^2\left(1+(1-2\kappa)^2\mu\right)}, \tag{B14}$$

$$\rho_{31} = \frac{Sin[\beta]\left(\left(-1-\kappa\mu + 2\kappa^{3/2}\lambda\mu + \sqrt{\kappa}(\lambda-\lambda\mu)\right) Cos[\beta] + (-1+\kappa)\lambda^2 \mathrm{Sin}[\beta] Tan[\beta]\right)}{1+\mu+\lambda^2\left(1+(1-2\kappa)^2\mu\right)}, \tag{B15}$$

$$\rho_{32} = \frac{\left(-1+\lambda^2+2\kappa^{3/2}\lambda\mu - \kappa\left(\lambda^2+\mu\right) + \sqrt{\kappa}(\lambda-\lambda\mu)\right) Sin[\beta]^2}{1+\mu+\lambda^2\left(1+(1-2\kappa)^2\mu\right)}, \tag{B16}$$

$$\rho_{33} = \frac{-(-1+\kappa)\mu Cos[\beta]^2 + \lambda\left(\sqrt{\kappa}(-1+\mu) - 2\kappa^{3/2}\mu + \lambda\mu + 4\kappa^2\lambda\mu + \kappa(\lambda-4\lambda\mu)\right) \mathrm{Sin}[\beta]^2}{1+\mu+\lambda^2\left(1+(1-2\kappa)^2\mu\right)}, \tag{B17}$$

$$\rho_{34} = -\frac{\left(\sqrt{\kappa}\lambda(-1+\mu) - 2\kappa^{3/2}\lambda\mu + 4\kappa^2\lambda^2\mu + \left(-1+\lambda^2\right)\mu + \kappa\left(\lambda^2(1-4\mu)+\mu\right)\right) Cos[\beta]\mathrm{Sin}[\beta]}{1+\mu+\lambda^2\left(1+(1-2\kappa)^2\mu\right)}, \tag{B18}$$

$$\rho_{41} = -\frac{\sqrt{\kappa}\lambda(1+(-1+2\kappa)\mu) Cos[\beta]^2 + \left(1+(-1+\kappa)\lambda^2+\kappa\mu\right) Sin[\beta]^2}{1+\mu+\lambda^2\left(1+(1-2\kappa)^2\mu\right)}, \tag{B19}$$

$$\rho_{42} = -\frac{Sin[\beta]\left(\lambda\left(\lambda - \kappa\lambda - \sqrt{\kappa}(-1+\mu) + 2\kappa^{3/2}\mu\right) Cos[\beta] + (1+\kappa\mu) Sin[\beta] Tan[\beta]\right)}{1+\mu+\lambda^2\left(1+(1-2\kappa)^2\mu\right)}, \tag{B20}$$

$$\rho_{43} = -\frac{Sin[\beta]\left(\left(4\kappa^2\lambda^2\mu + \left(\lambda^2-1\right)\mu + \kappa\left(\lambda^2+\mu-4\lambda^2\mu\right)\right) Cos[\beta] + \sqrt{\kappa}\lambda(1+(2\kappa-1)\mu) Sin[\beta] Tan[\beta]\right)}{1+\mu+\lambda^2\left(1+(1-2\kappa)^2\mu\right)}, \tag{B21}$$

$$\rho_{44} = \frac{\lambda^2\left(\kappa+\mu-4\kappa\mu+4\kappa^2\mu\right) Cos[\beta]^2 + \left(\mu - \kappa\mu + 2\kappa^{3/2}\lambda\mu + \sqrt{\kappa}(\lambda-\lambda\mu)\right) Sin[\beta]^2}{1+\mu+\lambda^2\left(1+(1-2\kappa)^2\mu\right)}. \tag{B22}$$

For $\beta = 0$, the solution is consistent with that in Eq. (B3).

Fig. B1 depicts the numerically obtained values of $Q_{\mathrm{E'A}}$ and the corresponding quantum Chernoff bounds P^M_{QCB} for $\beta = 0$, 0.05, 0.10, 0.15, 0.20, 0.25, and 0.30. Targets with both high and low reflectivity are examined. The average number of photons in mode B (before displacement $D(\beta)$) is $N_s = \frac{\lambda^2}{1-\lambda^2} = 0.10$. All the photons in each optical mode are truncated within the subspace of $\{|0\rangle, |1\rangle\}$, which is sufficient for studying quantum states with a small average number of photons. Particularly, both cases exhibit a pronounced decrease in $Q_{E'A}$ and in P^M_{QCB} for the large displacement β. Figs. B1(b) and (d) present P^M_{QCB} (in the logarithmic scale) as a function of the number of entangled states M for $\beta = 0, 0.05, 0.10 \cdots, 0.30$ (from top to bottom).

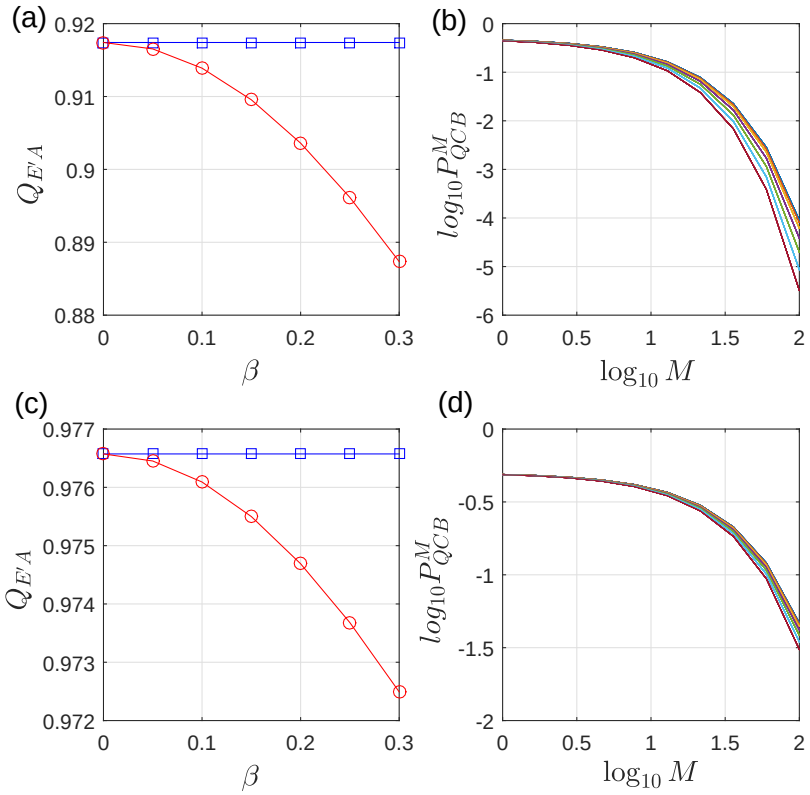

Figure B1 (Color online) Value of $Q_{E'A}$ and corresponding P^M_{QCB}. All quantum states are truncated in a 2D photon subspace spanned by $\{|0\rangle, |1\rangle\}$. For (a) and (b), we consider a target with high reflectivity ($\kappa_t = 0.7$), low-noise environment ($N_B = 0.1$), and signal strength of $N_s = 0.1$. For (c) and (d), we consider a low-reflectivity target in a noisy environment, such that $\kappa_t = 0.1, N_s = 0.1$, and $N_B = 0.1$. In (b) and (d), $\beta = 0, 0.05, 0.10, 0.15, 0.20, 0.25, and 0.30$ (from top to bottom).

Appendix B.2 High-noise conditions

The approximation of the 0-1 photon subspace only holds when the average number of photons is small. For a noisy environment with $N_B = \frac{\mu}{1-\mu} \gg 1$, the dimensions of the photon subspace required for faithful simulation increase rapidly. Thus, the phase space method needs to be implemented.

Generally, for any N-mode quantum system, each mode is an infinite dimensional subsystem and can be conveniently expressed using two field quadratures, i.e., the position operator $\hat{x}_i = (\hat{a}_i + \hat{a}_i^\dagger)/\sqrt{2}$ and momentum operator $\hat{p}_i = (\hat{a}_i - \hat{a}_i^\dagger)/(\imath\sqrt{2})$, where $\imath = \sqrt{-1}$ and $i = 1, 2, \cdots N$ denotes the index of the mode. $\hat{a}_i$ and $\hat{a}_i^\dagger$ represent the photon annihilation and creation operators for the i-th optical mode, respectively. For every density matrix ρ in Hilbert space, there is a corresponding characteristic function defined in the phase space $\chi(\mathbf{r}) = \mathrm{Tr}[\exp[\imath\hat{R}\mathbf{r}^{\mathrm{T}}]\rho]$, where $\hat{R} = (\hat{x}_1, \hat{p}_1, \hat{x}_2, \hat{p}_2 \cdots, \hat{x}_N, \hat{p}_N)$ and $\mathbf{r} \in \mathbb{R}^{2N}$ is a $2N$-dimensional real row vector. The Gaussian state is a special type of quantum state whose characteristic function is completely described by the covariance matrix and the average values of quadrature operators.

$$\chi(\mathbf{r}, V, \overline{\mathbf{R}}) = \exp\left[-\frac{1}{2}\mathbf{r}V\mathbf{r}^{\mathrm{T}} + \imath\overline{\mathbf{R}}\mathbf{r}^{\mathrm{T}}\right], \tag{B23}$$

where V is the $2N \times 2N$ covariance matrix,

$$\begin{aligned} &V_{lm} = \frac{1}{2}\mathrm{Tr}[(\hat{R}_l\hat{R}_m + \hat{R}_m\hat{R}_l)\rho] - \mathrm{Tr}[\hat{R}_l\rho]\mathrm{Tr}[\hat{R}_m\rho], \\ &l, m = 1, 2, 3, 4 \cdots, 2N, \end{aligned} \tag{B24}$$

and $\overline{\mathbf{R}}$ is the average value of quadrature operators $\hat{R}$.

The evolution of the unitary state, which is usually denoted with a unitary operator in the photon number space, can now be represented in terms of a symplectic operator $S \in \mathrm{SP}(2N, \mathbb{R})$ in the phase space:

$$V \to SVS^{\mathrm{T}}, \overline{\mathbf{R}} \to \overline{\mathbf{R}}S^{\mathrm{T}}, \tag{B25}$$

where V and $\overline{\mathbf{R}}$ are the covariance matrix and quadrature average of the density matrix ρ, respectively.

In Fig. A1(a), the input of modes A and B is a two-mode squeezed state (TMSS) and that of E is a thermal state, where the covariance matrix is given by V_{AB} and V_E:

$$V_{AB} = \frac{1}{2}\cosh(2r)I_4 + \frac{1}{2}\sinh(2r)\begin{pmatrix} 0 & 1 \\ 1 & 0 \end{pmatrix} \otimes \begin{pmatrix} 1 & 0 \\ 0 & -1 \end{pmatrix},$$

$$r = \mathrm{arctanh}(\lambda). \tag{B26}$$

$$V_E = (N_B + \frac{1}{2})I_2. \tag{B27}$$

In this study, I_2 and I_4 are 2-dimensional and 4-dimensional identity matrices, respectively.

In the phase space, the displacement operation on mode B induces a displacement in the quadrature average [4]. The quadrature of the three-mode state $E - A - B$ (before coupling at BS1) is

$$R_{EAB} = (0, 0) \oplus (0, 0, \sqrt{2}\beta, 0), \tag{B28}$$

and the covariance matrix is given by $V_{EAB} = V_E \oplus V_{AB}$.

The beam-splitter coupling between modes B and E can be expressed by a symplectic transformation:

$$S_{EB} = \begin{pmatrix} \sqrt{T} & & & & -\sqrt{1-T} & \\ & \sqrt{T} & & & & -\sqrt{1-T} \\ & & 1 & & & \\ & & & 1 & & \\ \sqrt{1-T} & & & & \sqrt{T} & \\ & \sqrt{1-T} & & & & \sqrt{T} \end{pmatrix}. \tag{B29}$$

After coupling, the three-mode Gaussian state in $E - A - B$ is expressed as

$$V'_{EAB} = S_{EB}(V_{EAB})S_{EB}^{\mathrm{T}}, \tag{B30}$$

$$R'_{EAB} = R_{EAB}S_{EB}^{\mathrm{T}}. \tag{B31}$$

Finally, the anti-displacement operation $D(-\beta)$ induces additional displacement on the quadrature, which yields

$$R''_{EAB} = R'_{EAB} + (-\sqrt{2}\beta, 0, 0, 0, 0, 0). \tag{B32}$$

The outgoing mode B is lost in the environment, and the final output state detected by the receiver is a two-mode Gaussian state; the quadrature average and covariance matrix of this output state are expressed as follows:

$$R''_{EA} = R''^{[1234]}_{EAB}, V''_{EA} = V^{[1234]}_{EAB}, \tag{B33}$$

where $R''^{[1234]}_{EAB}$ denotes the 1st, 2nd, 3rd, and 4th columns of R''_{EAB}, and $V^{[1234]}_{EAB}$ represents a submatrix consisting of the intersection of the 1st, 2nd, 3rd, and 4th rows and columns of matrix V_{EAB}.

By setting $\kappa = 0$ and $\kappa = \kappa_t$, the quadrature average and covariance matrix of the Gaussian state in both the absence ($\rho^{(0)}_{E'A}$) and presence ($\rho^{(1)}_{E'A}$) of the target can be obtained as follows:

$$V^{(0)}_{EA} = V''_{EA}|_{\kappa=0} = (N_B + \frac{1}{2})I_2 \oplus \frac{\cosh(2r)}{2} I_2, \tag{B34}$$

$$R^{(0)}_{EA} = R''_{EA}|_{\kappa=0} = (-\sqrt{2}\beta, 0, 0, 0), \tag{B35}$$

$$V^{(1)}_{EA} = V''_{EA}|_{\kappa=\kappa_t} = \begin{pmatrix} a_1 & & c_1 & \\ & a_1 & & -c_1 \\ c_1 & & \frac{\cosh(2r)}{2} & \\ & -c_1 & & \frac{\cosh(2r)}{2} \end{pmatrix}, \tag{B36}$$

$$c_1 = \frac{\sqrt{\kappa}\sinh(2r)}{2},$$

$$a_1 = \frac{\kappa\cosh(2r)}{2} + (1-\kappa)(N_B + \frac{1}{2}), \tag{B37}$$

$$R^{(1)}_{EA} = R''_{EA}|_{\kappa=\kappa_t} = (\sqrt{2}\beta(\sqrt{\kappa_t} - 1), 0, 0, 0). \tag{B38}$$

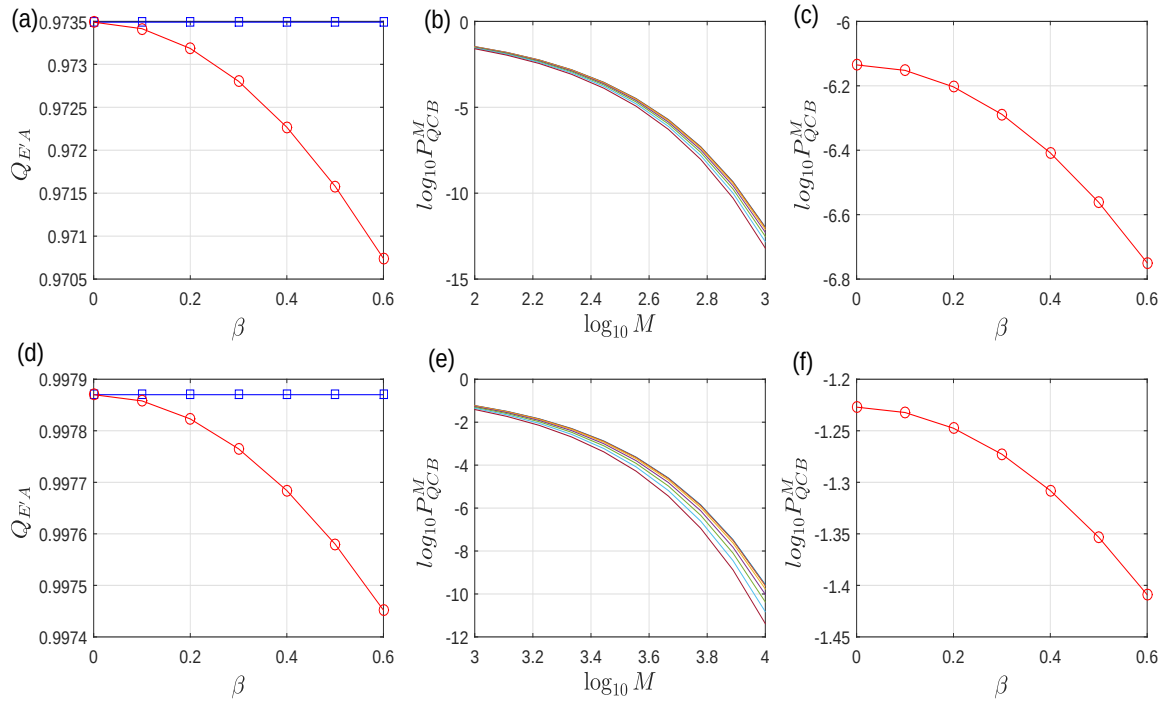

Figure B2 (Color online) Value of $Q_{E'A}$ and corresponding P^M_{QCB} for the high-reflectivity target (a, b, c) and low-reflectivity target (d, e, f). In (a), (b), and (c), we consider a target with $\kappa_t = 0.3$, high-noise environment ($N_B = 5$), and signal strength of $N_s = 0.5$. In (d), (e), and (f), we consider a low-reflectivity target hidden in a noisy environment, such that $\kappa_t = 0.05$, $N_s = 0.5$, and $N_B = 5$. In (b) and (e), $\beta = 0, 0.10, 0.20, 0.30, 0.40, 0.50, and 0.60$ from the top to bottom. In (b), (c): $M = 500$; in (e), (f): $M = 1000$.

To discriminate between the 2 two-mode Gaussian states with covariance matrix $V^{(0)}_{EA}, V^{(1)}_{EA}$ and quadrature average $R^{(0)}_{EA}, R^{(1)}_{EA}$, the quantum Chernoff bound should be used for the Gaussian states.

An easily computable bound for the discrimination between two n-mode Gaussian states has been reported in Ref. [5]. However, due to the difference in the definition of the covariance matrix (by a factor of 2), it is necessary to restate it according to the definition given in Eq. (B24).

Let us consider two arbitrary n-mode Gaussian states ρ_0 and ρ_1 with quadrature average $\bar{\mathbf{x}}_0, \bar{\mathbf{x}}_1$ and covariance matrix V_0, V_1. Let $\mathbf{S}_0, \{\alpha_k\}$ ($\mathbf{S}_1, \{\beta_k\}$) be the normal mode decompositions of V_0 and V_1, expressed as

$$V_0 = \mathbf{S}_0 \begin{pmatrix} \alpha_1 & & & & \\ & \alpha_1 & & & \\ & & \ldots & & \\ & & & \alpha_n & \\ & & & & \alpha_n \end{pmatrix} \mathbf{S}_0^{\mathrm{T}}, \tag{B39}$$

$$V_1 = \mathbf{S}_1 \begin{pmatrix} \beta_1 & & & & \\ & \beta_1 & & & \\ & & \ldots & & \\ & & & \beta_n & \\ & & & & \beta_n \end{pmatrix} \mathbf{S}_1^{\mathrm{T}}. \tag{B40}$$

Then, we have [5]

$$Q_s = \mathrm{Tr}[\rho_0^s \rho_1^{1-s}] = \bar{Q}_s \exp\left\{-\tfrac{1}{2}\mathbf{d}^T \left[\mathbf{V}_0(s) + \mathbf{V}_1(1-s)\right]^{-1} \mathbf{d}\right\}, \tag{B41}$$

where

$$\bar{Q}_s := \frac{2^n \prod_{k=1}^{n} G_s(2\alpha_k) G_{1-s}(2\beta_k)}{\sqrt{\det\left[\mathbf{V}_0(s) + \mathbf{V}_1(1-s)\right]}}. \tag{B42}$$

Here, $\mathbf{d} := \sqrt{2}(\bar{\mathbf{x}}_0 - \bar{\mathbf{x}}_1)$ and

$$\mathbf{V}_0(s) = \mathbf{S}_0 \left[\bigoplus_{k=1}^{n} \Lambda_s(2\alpha_k)\mathbf{I}_k\right] \mathbf{S}_0^T, \tag{B43}$$

$$\mathbf{V}_1(1-s) = \mathbf{S}_1 \left[\bigoplus_{k=1}^{n} \Lambda_{1-s}(2\beta_k)\mathbf{I}_k\right] \mathbf{S}_1^T, \tag{B44}$$

$$G_p(x) = \frac{2^p}{(x+1)^p - (x-1)^p}, \tag{B45}$$

$$\Lambda_p(x) = \frac{(x+1)^p + (x-1)^p}{(x+1)^p - (x-1)^p}. \tag{B46}$$

From Eq. (B34) and Eq. (B37), using a computable bound for the discrimination between two arbitrary Gaussian states [5], the values of $Q_{E'A}$ and the corresponding P_{QCB}^M can be easily determined.

Fig. B2 shows the decrease in $Q_{E'A}$ and that in the corresponding P_{QCB}^M when the target is hidden in a considerably noisy environment. We consider a case where the average number of photons in the noisy environment is $N_B = 5$, and a two-mode squeezed state (TMSS) with an average photon number of $N_s = 0.50$ is employed for target detection. We observe that the weak coherent state is enhanced with increasing β (= 0, 0.10, 0.20, 0.30, 0.40, 0.50, and 0.60). Furthermore, $Q_{E'A}$ is strictly dependent on the value of β, and the quantum Chernoff bound decreases as the amplitude of the displacement operation increases. To clarify how these displacement and anti-displacement operations improve quantum illumination, Fig. B2 (c) and (f) depict the dependence of error probability on displacement for $M = 500$ and $M = 1000$, respectively. At $\beta = 0$, the curves in (c) and (f) correspond to the early scheme in Fig. A1(a). The error probability (in the logarithmic scale) decreases monotonously as β increases. This implies that the displacement and anti-displacement aid in decreasing the errors in target detection.

The physical mechanisms underlying this enhancement in quantum illumination via the proposed approach need to be evaluated. As noted by Fuchs [6] and Nielsen [7], the trace distance is highly correlated with the error probability in quantum state discrimination; the larger the trace distance, the lower is the error probability. Hence, the decrease in error probability due to the displacement operation is likely associated with increments in the trace distance. This postulation can be verified by analyzing the trace distance of the quantum state $\delta(\rho_{E'A}^{(1)}, \rho_{E'A}^{(0)}) = \frac{1}{2}||\rho_{E'A}^{(1)} - \rho_{E'A}^{(0)}||$. For convenience, we consider a case where the background noise is $N_B = 1.0$, for which the truncation of the quantum state in the $D = 7$-dimensional subspace is sufficient. Subsequently, we choose $N_s = 0.5 and N_B = 1.0$ and also plot $\delta(\rho_{E'A}^{(1)}, \rho_{E'A}^{(0)})$ as a function of different displacements β, as shown in Fig. B3. From the figure, steady increments in the trace distance were noted for increasing values of β.

Appendix C Physical implementation of on-line displacement operation

Here, we show that the on-line displacement operation can be deterministically implemented using a beam splitter and ancillary coherent states. The on-line displacement scheme is presented in Fig. A1. Next, we use the phase space method to analyze the effects of displacement. We assume that BS2 is a beam splitter with a transmittance of T_0 and that the ancillary states in modes F and G are initialized as $|\beta_0\rangle$ and $|-\beta_0\rangle$, respectively.

The covariance matrix and quadrature average of the initial state $E - A - B - F - G$ can be expressed as

$$V_{EABFG}^{(1)} = \frac{1}{2}I_2 \oplus V_{AB} \oplus \frac{1}{2}I_2 \oplus \frac{1}{2}I_2, \tag{C1}$$

$$R_{EABFG}^{(1)} = \mathbf{0}_{1\times 6} \oplus (\sqrt{2}\beta_0, 0) \oplus (-\sqrt{2}\beta_0, 0). \tag{C2}$$

The coupling of the beam splitter at BS1 and BS2 can be formulated using symplectic transformations, as follows:

$$V_{EABFG}^{(2)} = S_{tot}(T_0) V_{EABFG}^{(1)} S_{tot}^{\mathrm{T}}, \tag{C3}$$

$$R_{EABFG}^{(2)} = R_{EABFG}^{(1)} S_{tot}^{\mathrm{T}}, \tag{C4}$$

$$S_{tot} = S_{EG}(T_0) S_{BE}(T) S_{BF}(T_0) \tag{C5}$$

As the optical mode $B - F - G$ is discarded, the final state used for signal detection is

$$R_{EA}^{out} = R_{EABFG}^{(2)[1234]}, V_{EA}^{out} = V_{EABFG}^{(2)[1234]}, \tag{C6}$$

where the symbol $^{[1234]}$ is as defined for Eq. (B33). Through direct calculation, we obtain

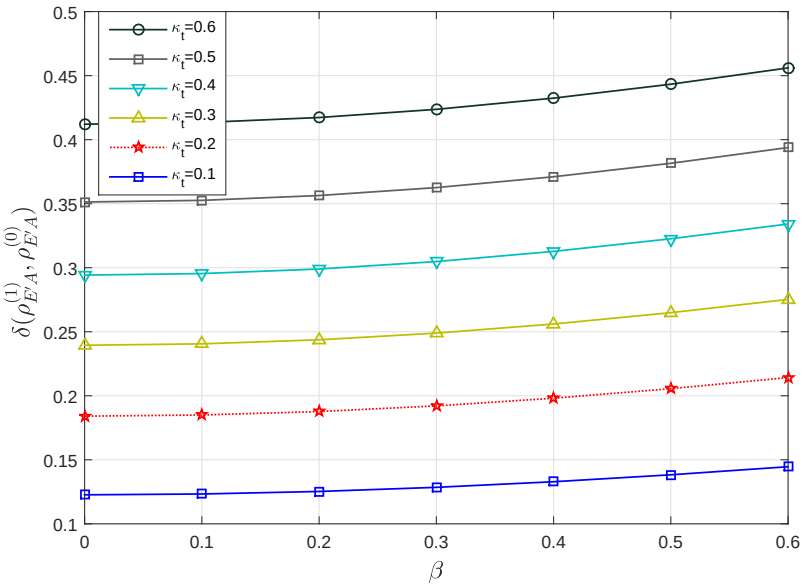

Figure B3 (Color online) Trace distance of $\delta(\rho^{(1)}_{E'A}, \rho^{(0)}_{E'A})$ as a function of β. The parameter κ_t is chosen as $\beta = 0.60, 0.50, 0.40, 0.30, 0.20, and 0.10$ (from the top to bottom). Other parameters are $N_s = 0.5 and N_B = 1.0$.

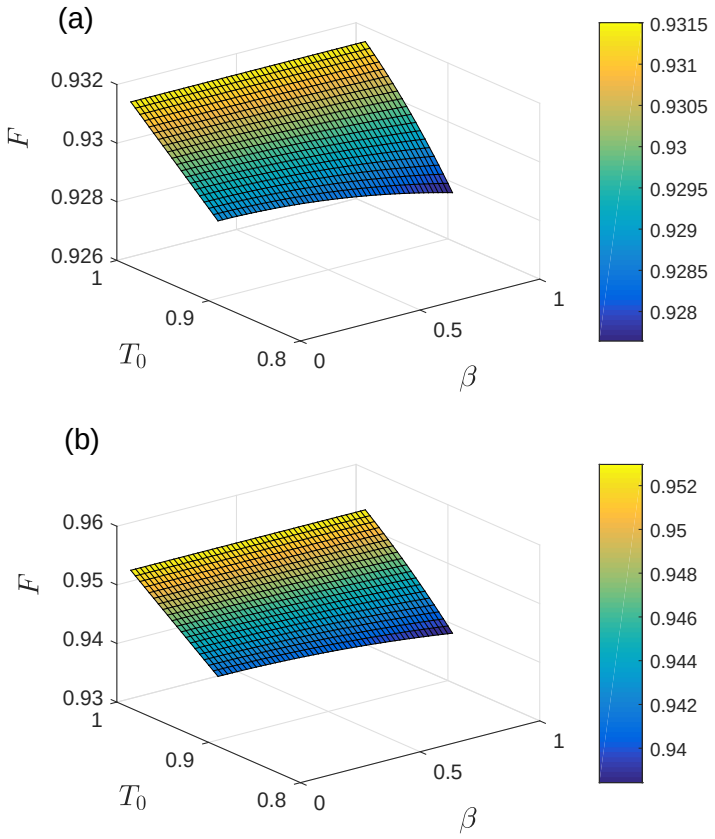

Figure C1 (Color online) Fidelity between the practical displacement scheme with the coherent state $|\beta_0\rangle$ ($\beta_0 = \beta/\sqrt{1-T_0}$) and beam splitter with transmittance T_0. Other parameters are (a) $N_s = 0.05$, $\kappa_t = 0.4$, and $N_B = 0.01$; and (b) $N_s = 0.08$, $\kappa_t = 0.99$, and $N_B = 2.0$.

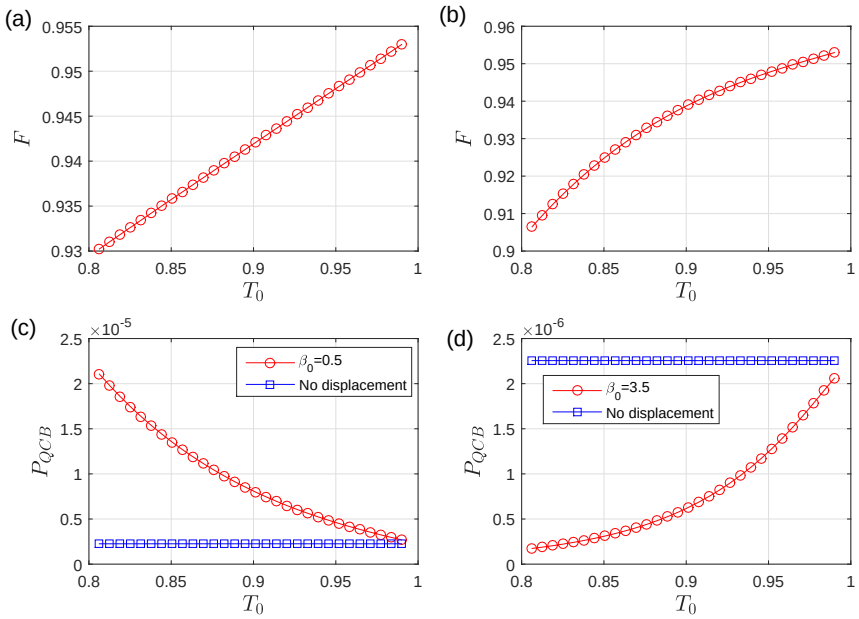

Figure C2 (Color online) (a) Fidelity and error probability P_{QCB}(c) as a function of the beam splitter transmittance T_0, for $\beta_0 = 0.5$. (b) Fidelity and error probability P_{QCB}(d) as a function of the beam splitter transmittance T_0, for $\beta_0 = 3.5$. Other parameters are $\kappa_t = 0.99$, $N_s = 0.08$, $N_B = 2, and M = 20$. The blue lines in (c) and (d) indicate the value of $P_{QCB} = 2.26 \times 10^{-6}$ when the displacement and anti-displacement operations are not used.

$$R_{EA}^{out} = (\sqrt{2}\beta_0\sqrt{1-T_0}(\sqrt{T_0\kappa}-1), 0, 0, 0), \tag{C7}$$

$$V_{EA}^{out} = \begin{pmatrix} a_2 & & c_2 & \\ & a_2 & & -c_2 \\ c_2 & & \frac{\cosh(2r)}{2} & \\ & -c_2 & & \frac{\cosh(2r)}{2} \end{pmatrix}, \tag{C8}$$

$$a_2 = \frac{1}{2}\left(1 + 2N_B T_0(1-\kappa) + {T_0}^2\kappa(-1+\cosh(2r))\right), \tag{C9}$$

$$c_2 = \frac{1}{2}T_0\sqrt{\kappa}\sinh(2r). \tag{C10}$$

Thus, by choosing the auxiliary coherent state $|\beta_0\rangle$ such that $\beta_0 = \beta/\sqrt{1-T_0}$ and $T_0 \to 1$, we obtain $R_{EA}^{out} \to R''_{EA}, V_{EA}^{out} \to V''_{EA}$, and the displacement operation is deterministically implemented. It should also be noted that the practical scheme with the beam splitter and the ancillary coherent state $|\beta_0\rangle$ induces a displacement in the quadrature average and a distortion in the covariance matrix. Generally, fidelity is used to evaluate the similarity between the two-mode Gaussian state in Eq. (C8) and that in Eq. (B36):

$$F = \frac{8}{\zeta}\exp[-\frac{8}{\zeta}(\sqrt{T_0}-1)^2\beta^2\kappa\cosh(2r)], \tag{C11}$$

$$\zeta = -4\left(-2 + 2N_B(1+T_0)(\kappa-1) + \kappa + {T_0}^2\kappa\right)\cosh(2r) + \kappa\left(3 + T_0(2+3T_0) + (T_0-1)^2\cosh(4r)\right). \tag{C12}$$

Fig. C1 shows the numerically calculated fidelity between the output states obtained via the joint measurement using the scheme in Fig. A1(b) and (d). In both low-noise and high-noise conditions, a fidelity of up to 0.92 can be achieved.

Generally, a higher fidelity indicates a more faithful implementation of the displacement and anti-displacement operations. However, fidelity is not completely equivalent to the error probability in quantum state discrimination, as the former evaluates the faithfulness of the on-line local displacement and anti-displacement operations, whereas the latter is more dependent on the distinguishability between two Gaussian states with quadrature averages and covariance matrices of $R_{EA}^{out}(\kappa=0), V_{EA}^{out}(\kappa=0)$ and $R_{EA}^{out}(\kappa=\kappa_t), V_{EA}^{out}(\kappa=\kappa_t)$, respectively. In Fig.C2(a) and (c), the fidelity and error probability in state discrimination are plotted for the same parameters $\kappa_t = 0.99$, $N_s = 0.08$, $N_B = 2, M = 20, and \beta_0 = 0.5$. It is evident that the fidelity exceeds 0.93 and increases monotonously when $T_0 > 0.80$. Moreover, the error probability decreases rapidly as T_0 increases. However, even at $T_0 = 0.99$, the error probability with the displacement operation is larger than that without the displacement and anti-displacement operations (blue lines in Fig.C2 (c)). This is because the practical displacement operation affects the quadrature average and also the covariance matrix (Eq.(C8)). The enhancement due to the practical displacement and anti-displacement operations is evident if a stronger displacement with $\beta_0 = 3.5$ is used. As shown in Fig.C2(b) and (d), the fidelity still exceeds 0.90 and increases as T_0 increases. Here, the error probability in state discrimination is further decreased for all $0.8 < T_0 < 1$. Particularly, for

$T_0 = 0.85$, the fidelity is $F = 0.92$, which is smaller than all the other fidelity values in Fig.C2(a). However, the error probability is $P_{QCB} = 3.11 \times 10^{-7}$, which is a decrease of approximately 86.2% compared to the value of $P_{QCB} = 2.26 \times 10^{-6}$ (blue lines) for cases without the displacement and anti-displacement operations.

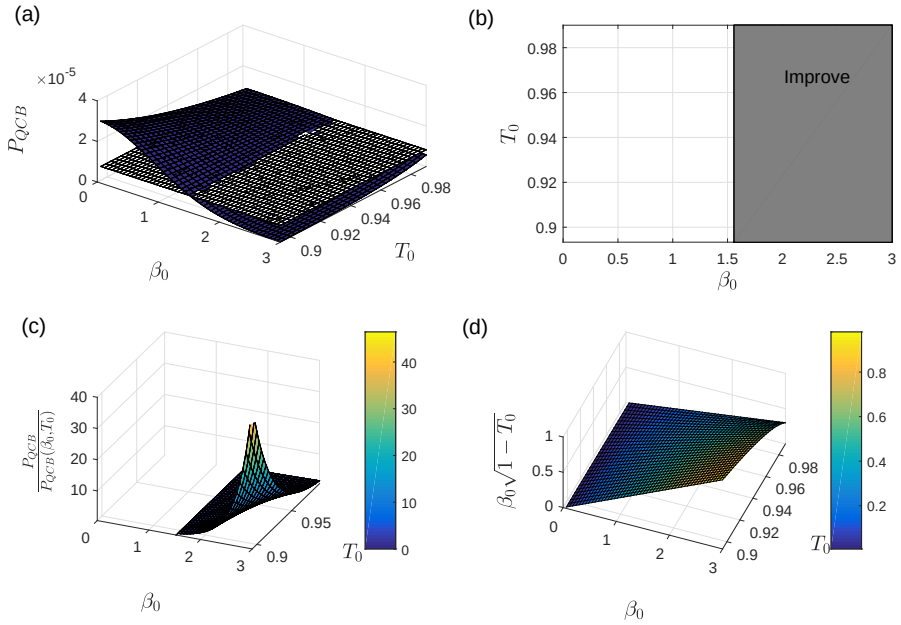

Figure C3 (Color online) (a) P_{QCB} as a function of the ancillary coherent state β_0 and transmittance of the beam splitter T_0. The gray plane indicates the value of $P_{QCB} = 8.26 \times 10^{-6}$ in the absence of displacement operation. (b) P_{QCB} decreases when $\beta_0 > 1.56$; the corresponding regime is indicated in gray. (c) Ratio between the error probability without displacement scheme and that with the displacement and anti-displacement operations. (d) Equivalent displacement $\beta_0\sqrt{1-T_0}$ as a function of β_0 and T_0. Other parameters are $\kappa_t = 0.2$, $N_s = 0.5$, $N_B = 2$, and $M = 500$.

The mechanisms underlying the enhancement caused by the application of the displacement and anti-displacement operations need to be examined in detail. Here, we use the phase space method and calculate the error probability P_{QCB}^{M} for several values of β_0 and T_0. We consider the case where $\kappa_t = 0.2$, $N_B = 2$, $N_s = 0.5$, and $M = 500$. It should be noted that the error probability is $P_{\mathrm{QCB}} = 8.26 \times 10^{-6}$ when displacement is absent. However, using the ancillary coherent states, the error probability can be further decreased when $\beta_0 > 1.56$. The corresponding regime in which the error probability is decreased is indicated in gray. Fig.C3(c) presents a plot of the ratio $\frac{P_{\mathrm{QCB}}}{P_{\mathrm{QCB}}(\beta_0,T_0)}$ for $0 < \beta_0 < 3$ and $0.89 < T_0 < 0.99$. Under the condition $\beta_0 > 1.56$, the aforementioned ratio is always greater than one, indicating that the error probability decreases if the practical scheme shown in Fig.A1 (d) is used. Specifically, for $\beta_0 = 3.0 and T_0 = 0.89$, the ratio is equal to 46.4, implying that the reduced probability is only one in forty-six for the original scheme without displacement and anti-displacement operations. Fig.C3(d) presents an evaluation of the displacement for β_0 and T_0. The maximum displacement occurs at $\beta_0 = 3.0 and T_0 = 0.89$, which is consistent with our primary conclusion, i.e., a larger displacement induces a more pronounced decrease in P_{QCB}.

References

1 Sacchi M F, Optimal discrimination of quantum operations, Phys. Rev. A 2005, 71, 062340
2 Sacchi M F, Entanglement can enhance the distinguishability of entanglement-breaking channels, Phys. Rev. A, 2005 72, 014305
3 Guha S and Erkmen B I, Gaussian-state quantum-illumination receivers for target detection, Phys. Rev. A 2009 80, 052310
4 Walls D F and Milburn G J, in *Quantum Optics,* (Springer-Verlag, 1994).
5 Pirandola S and Lloyd S, Computable bounds for the discrimination of gaussian states, Phys. Rev. A 2008, 78, 012331
6 Christopher A F, Distinguishability and Accessible Information in Quantum Theory, Ph. D. Dissertation, University of New Mexico.
7 Gilchrist A, Langford N K, and Nielsen M A, Distance measures to compare real and ideal quantum processes, Phys. Rev. A 2005, 71, 062310